

Document downloaded from:

<http://hdl.handle.net/10251/46951>

This paper must be cited as:

Li ., L.; Zhou ., H.; Franssen, H.; Gómez-Hernández, JJ. (2012). Modeling transient groundwater flow by coupling ensemble Kalman filtering and upscaling. *Water Resources Research*. 48(1):1-19. doi:10.1029/2010WR010214.



The final publication is available at

<http://dx.doi.org/10.1029/2010WR010214>

Copyright American Geophysical Union (AGU)

¹ Modeling Transient Groundwater Flow by Coupling ² Ensemble Kalman Filtering and Upscaling

Liangping Li,^{1,2} Haiyan Zhou,^{1,2} Harrie-Jan Hendricks Franssen³ and J.

Jaime Gómez-Hernández,²

Liangping Li and Haiyan Zhou, School of Water Resources and Environment, China University of Geosciences (Beijing), Beijing 100083, China.

Liangping Li, Haiyan Zhou and Jaime Gómez-Hernández, Group of Hydrogeology, Universitat Politècnica de València, Camino de Vera, s/n, 46022 Valencia, Spain. (liali@upvnet.upv.es)

Harrie-Jan Hendricks Franssen, Agrosphere, ICG-4, Forschungszentrum Jülich GmbH, Germany

¹School of Water Resources and Environment, China University of Geosciences (Beijing), China

²Group of Hydrogeology, Universitat Politècnica de València, Spain

³Agrosphere, ICG-4, Forschungszentrum Jülich GmbH, Germany

Abstract. The ensemble Kalman filter (EnKF) is coupled with upscaling to build an aquifer model at a coarser scale than the scale at which the conditioning data (conductivity and piezometric head) had been taken for the purpose of inverse modeling. Building an aquifer model at the support scale of observations is most often impractical, since this would imply numerical models with millions of cells. If, in addition, an uncertainty analysis is required involving some kind of Monte-Carlo approach, the task becomes impossible. For this reason, a methodology has been developed that will use the conductivity data, at the scale at which they were collected, to build a model at a (much) coarser scale suitable for the inverse modeling of groundwater flow and mass transport. It proceeds as follows: (i) generate an ensemble of realizations of conductivities conditioned to the conductivity data at the same scale at which conductivities were collected, (ii) upscale each realization onto a coarse discretization; on these coarse realizations, conductivities will become tensorial in nature with arbitrary orientations of their principal directions, (iii) apply the EnKF to the ensemble of coarse conductivity upscaled realizations in order to condition the realizations to the measured piezometric head data. The proposed approach addresses the problem of how to deal with tensorial parameters, at a coarse scale, in ensemble Kalman filtering, while maintaining the conditioning to the fine scale hydraulic conductivity measurements. We demonstrate our approach in the framework of a synthetic worth-of-data exercise, in which the relevance of conditioning to conductivities, piezometric heads or both is analyzed.

1. Introduction

26 In this paper we address two problems, each of which has been the subject of many
27 works, but which have not received as much attention when considered together: upscaling
28 and inverse modeling. There are many reviews on the importance and the methods of
29 upscaling [e.g., *Wen and Gómez-Hernández*, 1996; *Renard and de Marsily*, 1997; *Sánchez-*
30 *Vila et al.*, 2006], and there are also many reviews on inverse modeling and its relevance
31 for aquifer characterization [e.g., *Yeh*, 1986; *McLaughlin and Townley*, 1996; *Zimmerman*
32 *et al.*, 1998; *Carrera et al.*, 2005; *Hendricks Franssen et al.*, 2009; *Oliver and Chen*, 2011;
33 *Zhou et al.*, 2011a]. Our interest lies in coupling upscaling and inverse modeling to perform
34 an uncertainty analysis of flow and transport in an aquifer for which measurements have
35 been collected at a scale so small that it is prohibitive, if not impossible, to perform
36 directly the inverse modeling.

37 The issue of how to reconcile the scale at which conductivity data are collected and the
38 scale at which numerical models are calibrated was termed “the missing scale” by *Tran*
39 [1996], referring to the fact that the discrepancy between scales was simply disregarded;
40 data were collected at a fine scale, the numerical model was built at a much larger scale,
41 each datum was assigned to a given block, and the whole block was assigned the datum
42 value, even though the block may be several orders of magnitude larger than the volume
43 support of the sample. This procedure induced a variability, at the numerical block
44 scale, much larger than it should be, while at the same time some unresolved issues have
45 prevailed like what to do when several samples fell in the same block.

46 To the best of our knowledge, the first work to attempt the coupling of upscaling and in-
47 verse modeling is the upscaling-calibration-downscaling-upscaling approach by *Tran et al.*
48 [1999]. In their approach, a simple averaging over a uniformly coarsened model is used
49 to upscale the hydraulic conductivities. Then, the state information (e.g., dynamic piezo-
50 metric head data) is incorporated in the upscaled model by the self-calibration technique
51 [*Gómez-Hernández et al.*, 1997]. The calibrated parameters are downscaled back to the
52 fine scale by block kriging [*Behrens et al.*, 1998] resulting in a fine scale realization condi-
53 tional to the measured parameters (e.g., hydraulic conductivities). Finally, the downscaled
54 conductivities are upscaled using a more precise scheme [*Durlofsky et al.*, 1997; *Li et al.*,
55 2011a] for prediction purposes. The main shortcoming of this approach is that the in-
56 verse modeling is performed on a crude upscaled model, resulting in a downscaled model
57 that will not honor the state data accurately. *Tureyen and Caers* [2005] proposed the
58 calibration of the fine scale conductivity field by gradual deformation [*Hu*, 2000; *Capilla*
59 *and Llopis-Albert*, 2009], but instead of solving the flow equation at the fine scale they
60 used an approximate solution after upscaling the hydraulic conductivity field to a coarse
61 scale. This process requires an upscaling for each iteration of the gradual deformation
62 algorithm, which is also time-consuming, although they avoid the fine scale flow solution.
63 More recently, an alternative multiscale inverse method [*Fu et al.*, 2010] was proposed. It
64 uses a multiscale adjoint method to compute sensitivity coefficients and reduce the compu-
65 tational cost. However, like traditional inverse methods, the proposed approach requires
66 a large amount of CPU time in order to get an ensemble of conditional realizations. In
67 our understanding, nobody has attempted to couple upscaling and the ensemble Kalman
68 filtering (EnKF) for generating hydraulic conductivity fields conditioned to both hydraulic

69 conductivity and piezometric head measurements. Only the work by *Peters et al.* [2010]
70 gets close to our work as. For the Brugge Benchmark Study, they generated a fine scale
71 permeability field, which was upscaled using a diagonal tensor upscaling. The resulting
72 coarse scale model was provided to the different teams participating in the benchmark
73 exercise, some of which used the EnKF for history matching. We have chosen the EnKF
74 algorithm for the inverse modeling because it has been shown that it is faster than other
75 alternative Monte Carlo-based inverse modeling methods (see for instance the work by
76 *Hendricks Franssen and Kinzelbach* [2009] who show that the EnKF was 80 times faster
77 than the sequential self-calibration in a benchmark exercise and nearly as good).

78 Our aim is to propose an approach for the stochastic inverse modeling of an aquifer that
79 has been characterized at a scale at which it is impossible to solve the inverse problem, due
80 to the large number of cells needed to discretize the domain. We start with a collection of
81 hydraulic conductivity and piezometric head measurements, taken at a very small scale,
82 to end with an ensemble of hydraulic conductivity realizations, at a scale much larger
83 than the one at which data were originally sampled, all of which are conditioned to the
84 measurements. This ensemble of realizations will serve to perform uncertainty analyses of
85 both the parameters (hydraulic conductivities) and the system state variables (piezometric
86 heads, fluxes, concentrations, or others).

87 The rest of the paper is organized as follows. Section 2 outlines the coupling of upscaling
88 and the EnKF, with emphasis in the use of arbitrary hydraulic conductivity tensors in the
89 numerical model. Next, in section 3, a synthetic example serves to validate the proposed
90 method. Then, in section 4, the results are discussed. The paper ends with a summary
91 and conclusions.

2. Methodology

92 Hereafter, we will refer to a fine scale for the scale at which data are collected, and
93 a coarse scale, for the scale at which the numerical models are built. The methodology
94 proposed can be outlined as follows:

95 1. At the fine scale, generate an ensemble of realizations of hydraulic conductivity
96 conditioned to the hydraulic conductivity measurements.

97 2. Upscale each one of the fine scale realizations generated in the previous step. In the
98 most general case, the upscaled conductivities will be full tensors in the reference axes.

99 3. Use the ensemble of coarse realizations with the EnKF to condition (assimilate) on
100 the measured piezometric heads.

2.1. Generation of the Ensemble of Fine Scale Conductivities

101 The first step of the proposed methodology makes use of geostatistical tools already
102 available in the literature [e.g., *Gómez-Hernández and Srivastava, 1990; Deutsch and*
103 *Journal, 1998; Strebelle, 2002; Mariethoz et al., 2010*]. The technique to choose will
104 depend on the underlying random function model selected for the hydraulic conductivity:
105 multi-Gaussian, indicator-based, pattern-based, or others. In all cases, the scale at which
106 these fields can be generated is not an obstacle, and the resulting fields will be conditioned
107 to the measured hydraulic conductivity measurements (but only to hydraulic conductivity
108 measurements). These fields could have millions of cells and are not suitable for inverse
109 modeling of groundwater flow and solute transport.

2.2. Upscaling

Each one of the realizations generated in the previous step is upscaled onto a coarse grid with a number of blocks sufficiently small for numerical modeling. We use the flow upscaling approach by *Rubin and Gómez-Hernández* [1990] who, after spatially integrating Darcy's law over a block V ,

$$\frac{1}{V} \int_V \bar{\mathbf{q}} dV = -\mathbf{K}^b \left(\frac{1}{V} \int_V \nabla \bar{\mathbf{h}} dV \right), \quad (1)$$

110 define the block conductivity tensor (\mathbf{K}^b) as the tensor that best relates the block average
 111 head gradient ($\nabla \bar{\mathbf{h}}$) to the block average specific discharge vector ($\bar{\mathbf{q}}$) within the block.
 112 Notice that to perform the two integrals in the previous expressions we need to know the
 113 specific discharge vectors and the piezometric head gradients at the fine scale within the
 114 block. These values could be obtained after a solution of the flow problem at the fine scale
 115 [i.e., *White and Horne*, 1987], but this approach beats the whole purpose of upscaling,
 116 which is to avoid such fine scale numerical simulations. The alternative is to model a
 117 smaller domain of the entire aquifer enclosing the block being upscaled. In such a case,
 118 the boundary conditions used in this reduced model will be different from the boundary
 119 conditions that the block has in the global model, and this will have some impact on the
 120 fine scale values of $\nabla \bar{\mathbf{h}}$ and $\bar{\mathbf{q}}$. The dependency of the heads and flows within the block
 121 on the boundary conditions is the reason why the block upscaled tensor is referred to as
 122 non-local [e.g., *Indelman and Abramovich*, 1994; *Guadagnini and Neuman*, 1999].

123 For the flow upscaling we adopt the so-called Laplacian-with-skin method on block inter-
 124 faces as described by *Gómez-Hernández* [1991] and recently extended to three dimensions
 125 by *Zhou et al.* [2010]. The two main advantages of this approach are that it can handle
 126 arbitrary full conductivity tensors, without any restriction on their principal directions;
 127 and that it upscales directly the volume straddling between adjacent block centers, which,

128 at the end, is the parameter used in the standard finite-difference approximation of the
129 groundwater flow equation (avoiding the derivation of this value by some kind of averaging
130 of the adjacent block values). Once the interblock conductivities have been computed, a
131 specialized code capable of handling interblock tensors is necessary. For this purpose, the
132 public domain code FLOWXYZ3D [Li et al., 2010], has been developed. The details of
133 the upscaling approach, the numerical modeling using interblock conductivity tensors, and
134 several demonstration cases can be found in Zhou et al. [2010]; Li et al. [2010, 2011a, b].
135 The resulting upscaled interblock tensors produced by this approach are always of rank
136 two, symmetric and positive definite.

137 The Laplacian-with-skin method on block interfaces for a given realization can be briefly
138 summarized as follows:

- 139 • Overlay a coarse grid on the fine scale hydraulic conductivity realization.
- 140 • Define the interblock volumes that straddle any two adjacent blocks.
- 141 • For each interblock:
 - 142 – Isolate the fine scale conductivities within a volume made up by the interblock plus
143 an additional “border ring” or “skin” and simulate flow, at the fine scale, within this
144 volume.
 - 145 – As explained in many studies [e.g, Gómez-Hernández, 1991; Sánchez-Vila et al.,
146 1995; Sánchez-Vila et al., 2006; Zhou et al., 2010; Li et al., 2011a], there is a need to solve
147 more than one flow problem in order to being able of identifying all components of the
148 interblock conductivity tensor.
 - 149 – From the solution of the flow problems, use Equation (1) to derive the interblock
150 conductivity tensor.

- 151 • Assemble all interblock tensors to build a realization of upscaled hydraulic conduc-
152 tivity tensors at the coarse scale.

153 The above procedure has to be repeated for all realizations, ending up with an ensemble
154 of realizations of interblock conductivity tensors.

2.3. The EnKF with Hydraulic Conductivity Tensors

155 Extensive descriptions of the EnKF and how to implement it have been given, for
156 instance, by *Burgers et al.* [1998]; *Evensen* [2003]; *Naevdal et al.* [2005]; *Chen and Zhang*
157 [2006]; *Aanonsen et al.* [2009]. Our contribution, regarding the EnKF, is how to deal
158 with an ensemble of parameters that, rather than being scalars, are tensors. After testing
159 different alternatives, we finally decided not to use the tensor components corresponding
160 to the Cartesian reference system as parameters within the EnKF, but to use some of
161 the tensor invariants, more precisely, the magnitude of the principal components and the
162 angles that define their orientation.

For the example discussed later we will assume a two-dimensional domain, with hy-
draulic conductivity tensors varying in space $\mathbf{K} = \mathbf{K}(\mathbf{x})$ of the form

$$\mathbf{K} = \begin{bmatrix} K_{xx} & K_{xy} \\ K_{xy} & K_{yy} \end{bmatrix}. \quad (2)$$

163 Each conductivity tensor is converted onto a triplet $\{K_{max}, K_{min}, \theta\}$, with K_{max} being the
164 largest principal component, K_{min} , the smallest one, and θ , the orientation, of the maxi-
165 mum principal component with respect to the x -axis according to the following expressions

166 [Bear, 1972]:

$$\begin{aligned}
 K_{max} &= \frac{K_{xx} + K_{yy}}{2} + \left[\left(\frac{K_{xx} - K_{yy}}{2} \right)^2 + (K_{xy})^2 \right]^{1/2}, \\
 K_{min} &= \frac{K_{xx} + K_{yy}}{2} - \left[\left(\frac{K_{xx} - K_{yy}}{2} \right)^2 + (K_{xy})^2 \right]^{1/2}, \\
 \theta &= \frac{1}{2} \arctan \left(\frac{2K_{xy}}{K_{xx} - K_{yy}} \right).
 \end{aligned} \tag{3}$$

167 After transforming all conductivity tensors obtained in the upscaling step onto their
 168 corresponding triplets, we are ready to apply the EnKF. We will use the EnKF im-
 169 plementation with an augmented state vector as discussed below; this is the standard
 170 implementation used in petroleum engineering and hydrogeology, although alternative
 171 implementations and refinements of the algorithm could have been used [see *Aanonsen*
 172 *et al.*, 2009, for a review].

Using the EnKF nomenclature, the state of the system is given by the spatial distribu-
 tion of the hydraulic heads, the state transition equation is the standard flow equation
 describing the movement of an incompressible fluid in a fully saturated porous medium
 [Bear, 1972; Freeze and Cherry, 1979] (in two dimensions for the example considered
 later), and the parameters of the system are the spatially varying hydraulic conductivities
 (the storage coefficient is assumed to be homogeneous and known, and therefore, it is a
 parameter not subject to filtering), i.e.,

$$\mathbf{Y}_k = f(\mathbf{X}_{k-1}, \mathbf{Y}_{k-1}), \tag{4}$$

173 where \mathbf{Y}_k is the state of the system at time step t_k , f represents the groundwater flow
 174 model (including boundary conditions, external stresses, and known parameters), and
 175 \mathbf{X}_{k-1} represents the model parameters after the latest update at time t_{k-1} .

176 The EnKF algorithm will proceed as follows:

177 1. Forecast. Equation (4) is used to forecast the system states for the next time step
 178 given the latest state and the latest parameter update. This forecast has to be performed
 179 in all realizations of the ensemble.

180 2. Analysis. At the forecasted time step, new state observations are available at mea-
 181 surement locations. The discrepancy between these state observations and the forecasted
 182 values will serve to update both the parameter values and the system state at all locations
 183 in the aquifer model as follows:

(i) Build the joint vector Ψ_k , including parameters and state values. This vector can
 be split into as many members as there are realizations in the ensemble, with

$$\Psi_{k,j} = \begin{bmatrix} \mathbf{X} \\ \mathbf{Y} \end{bmatrix}_{k,j} \quad (5)$$

being the j^{th} ensemble member at time t_k . Specifically, \mathbf{X} (for a realization) is expressed
 as:

$$\mathbf{X} = [(\ln K_{max}, \ln K_{min}, \theta)_1, \dots, (\ln K_{max}, \ln K_{min}, \theta)_{N_b}]^T \quad (6)$$

184 where N_b is the number of interfaces in the coarse numerical model. Notice that the
 185 logarithm of the conductivity principal components is used, since their distribution is,
 186 generally, closer to Gaussian than that of the conductivities themselves, which results
 187 in the optimality in the performance of the EnKF [*Evensen, 2003; Zhou et al., 2011b;*
 188 *Schöniger et al., 2011*].

(ii) The joint vector Ψ_k is updated, realization by realization, by assimilating the
 observations (\mathbf{Y}_k^{obs}):

$$\Psi_{k,j}^a = \Psi_{k,j}^f + \mathbf{G}_k \left(\mathbf{Y}_k^{obs} + \epsilon - \mathbf{H}\Psi_{k,j}^f \right), \quad (7)$$

where the superscripts a and f denote analysis and forecast, respectively; ϵ is a random observation error vector; \mathbf{H} is a linear operator that interpolates the forecasted heads to the measurement locations, and, in our case, is composed of 0's and 1's since we assume that measurements are taken at block centers. Therefore, equation (7) can be rewritten as:

$$\Psi_{k,j}^a = \Psi_{k,j}^f + \mathbf{G}_k \left(\mathbf{Y}_k^{obs} + \epsilon - \mathbf{Y}_{k,j}^f \right), \quad (8)$$

where the Kalman gain \mathbf{G}_k is given by:

$$\mathbf{G}_k = \mathbf{P}_k^f \mathbf{H}^T \left(\mathbf{H} \mathbf{P}_k^f \mathbf{H}^T + \mathbf{R}_k \right)^{-1}, \quad (9)$$

189 where \mathbf{R}_k is the measurement error covariance matrix, and \mathbf{P}_k^f contains the covariances
 190 between the different components of the state vector. \mathbf{P}_k^f is estimated from the ensemble
 191 of forecasted states as:

$$\begin{aligned} \mathbf{P}_k^f &\approx E \left[\left(\Psi_{k,j}^f - \overline{\Psi}_{k,j}^f \right) \left(\Psi_{k,j}^f - \overline{\Psi}_{k,j}^f \right)^T \right] \\ &\approx \sum_{j=1}^{N_e} \frac{\left(\Psi_{k,j}^f - \overline{\Psi}_{k,j}^f \right) \left(\Psi_{k,j}^f - \overline{\Psi}_{k,j}^f \right)^T}{N_e}, \end{aligned} \quad (10)$$

192 where N_e is the number of realizations in the ensemble, and the overbar denotes average
 193 through the ensemble.

194 In the implementation of the algorithm, it is not necessary to calculate explicitly the full
 195 covariance matrix \mathbf{P}_k^f , since the matrix \mathbf{H} is very sparse, and, consequently, the matrices
 196 $\mathbf{P}_k^f \mathbf{H}^T$ and $\mathbf{H} \mathbf{P}_k^f \mathbf{H}^T$ can be computed directly at a strongly reduced CPU cost.

197 3. The updated state becomes the current state, and the forecast-analysis loop is started
 198 again.

199 The question remains whether the updated conductivity-tensor realizations preserve the
 200 conditioning to the fine scale conductivity measurements. In standard EnKF, when no up-

201 scaling is involved and conductivity values are the same in all realizations at conditioning
202 locations, the forecasted covariances and cross-covariances involving conditioning points
203 are zero, and so is the Kalman gain at those locations; therefore, conductivities remain
204 unchanged through the entire Kalman filtering. In our case, after upscaling the fine-scale
205 conditional realizations, the resulting ensemble of hydraulic conductivity tensor realiza-
206 tions will display smaller variances (through the ensemble) for the tensors associated with
207 interfaces close to the fine scale measurements than for those far from the measurements.
208 These smaller variances will result in a smaller Kalman gain in the updating process at
209 these locations, and therefore will induce a soft conditioning of the interblock tensors on
210 the fine scale measurements.

211 The proposed method is implemented in the C software Upscaling-EnKF3D, which is
212 used in conjunction with the finite-difference program FLOWXYZ3D [*Li et al.*, 2010] in the
213 forecasting step. From an operational point of view, the proposed approach is suitable for
214 parallel computation both in terms of upscaling and EnKF, since each ensemble member
215 is treated independently, except for the computation of the Kalman gain.

2.4. CPU time analysis

216 Without a CPU analysis, we can argue that the coupling of upscaling with the EnKF
217 is of interest because it allows to analyze problems that otherwise could not be handled
218 simply because the size of the numerical model is not amenable to the available computer
219 resources. In our case, with our resources, we could not run any flow model with more
220 than 10^8 nodes. However, even for those models for which we could run the fine scale flow
221 simulation, the CPU time savings associated to the upscaling approach are considerable

222 and worth considering for fine scale models with more than a few tens of thousands of
 223 nodes.

224 We performed a conservative analysis of CPU time savings in which only the CPU time
 225 spent in the flow simulations is considered, the savings will be larger when the time needed
 226 to estimate the ensemble covariance and the Kalman gain are considered. We run several
 227 flow simulations for model sizes ranging from 10^4 to 10^7 nodes, for different realizations
 228 of the hydraulic conductivities with the same statistical characteristics as the examples
 229 that will be shown later. The regression of the CPU times with respect to the number of
 230 nodes (Figure 1) gives the following expression:

$$CPUt = 10^{-5}N_{cells} \quad (11)$$

231 A conservative CPU time analysis has been performed in order to

3. Application Example

232 In this section, a synthetic experiment illustrates the effectiveness of the proposed cou-
 233 pling of EnKF and upscaling.

3.1. Reference Field

234 We generate a realization of hydraulic conductivity over a domain discretized into 350
 235 by 350 cells of 1 m by 1 m using the code GCOSIM3D [*Gómez-Hernández and Journel,*
 236 1993].

We assume that, at this scale, conductivity is scalar and its natural logarithm, $\ln K$, can be characterized by a multiGaussian distribution of mean -5 (ln cm/s) and unit variance, with a strong anisotropic spatial correlation at the 45° orientation. The correlation range

in the largest continuity direction (x') is $\lambda_{x'} = 90$ m and in the smallest continuity direction (y') is $\lambda_{y'} = 18$ m. The Gaussian covariance function is given by:

$$\gamma(\mathbf{r}) = 1.0 \cdot \left\{ 1 - \exp \left[- \sqrt{\left(\frac{3r_{x'}}{90}\right)^2 + \left(\frac{3r_{y'}}{18}\right)^2} \right] \right\}, \quad (12)$$

with

$$\begin{bmatrix} r_{x'} \\ r_{y'} \end{bmatrix} = \begin{bmatrix} 1/\sqrt{2} & 1/\sqrt{2} \\ -1/\sqrt{2} & 1/\sqrt{2} \end{bmatrix} \begin{bmatrix} r_x \\ r_y \end{bmatrix}, \quad (13)$$

and $r = (r_x, r_y)$ being the separation vector in Cartesian coordinates. The reference realization is shown in Figure 4A. From this reference realization 100 conductivity data are sampled at the locations shown in Figure 4B. These data will be used for conditioning.

The forward transient groundwater flow model is run in the reference realization with the boundary conditions shown in Figure 5 and initial heads equal to zero everywhere. The total simulation time is 500 days, discretized into 100 time steps following a geometric sequence of ratio 1.05. The aquifer is confined. Specific storage is assumed constant and equal to 0.003 m^{-1} . The simulated piezometric heads at the end of time step 60 (67.7 days) are displayed in Figure 6. Piezometric heads at locations W1 to W9 in Figure 5 are sampled for the first 60 time steps to be used as conditioning data. The simulated heads at locations W10 to W13 will be used as validation data.

3.2. Hydraulic Conductivity Upscaling

For the reasons explained by *Zhou et al.* [2010]; *Li et al.* [2010], the fine scale realizations must be slightly larger than the aquifer domain in order to apply the Laplacian-with-skin upscaling approach. We assume that the aquifer of interest is comprised by the inner 320 by 320 cell domain for all realizations. Each one of these realizations is upscaled onto a 32 by 32 square-block model implying an order-of-two magnitude reduction in the

253 discretization of the aquifer after upscaling. After several tests, the skin selected for the
254 upscaling procedure has a width of 10 m, since it is the one that gives best results in the
255 reproduction of the interblock specific discharges when compared to those computed on
256 the fine scale underlying realizations.

257 Since the upscaling is applied to the interblock volume straddling between adjacent
258 block centers, there are 32 by 31 column-to-column interblock tensors ($\mathbf{K}^{b,c}$) plus 31 by
259 32 row-to-row interblock tensors ($\mathbf{K}^{b,r}$). All interblock tensors are transformed into their
260 corresponding triplet of invariants prior to starting the EnKF algorithm.

261 For illustration purposes, Figure 7 shows the resulting triplets for the reference field.
262 This figure will be used later as the reference upscaled field to analyze the performance
263 of the proposed method. On the right side of Figure 6, the simulated piezometric heads
264 at the end of the 60th time step are displayed side by side with the simulated piezometric
265 heads at the fine scale. The reproduction of the fine scale spatial distribution by the
266 coarse scale simulation is, as can be seen, very good; the average absolute discrepancy
267 between the heads at the coarse scale and heads at the fine scale (on the block centers) is
268 only 0.087 m.

3.3. Case Studies

269 Four cases, considering different types of conditioning information, are analyzed to
270 study the performance of the proposed approach (see Table 1). They will show that
271 the coupling of the EnKF with upscaling can be used to construct aquifer models that
272 are conditional to conductivity and piezometric head data, when there is an important
273 discrepancy between the scale at which the data are collected and the scale at which the
274 flow model is built. The cases will serve also to carry out a standard worth-of-data exercise

275 in which we analyze the trade-off between conductivity data and piezometric head data
276 regarding aquifer characterization.

277 Case A is unconditional, 200 realizations are generated according to the spatial corre-
278 lation model given by Equation (11) at the fine scale. Upscaling is performed in each
279 realization and the flow model is run. No Kalman filtering is performed.

280 Case B is conditional to logconductivity measurements, 200 realizations of logconduc-
281 tivity conditional to the 100 logconductivity measurements of Figure 3B are generated at
282 the fine scale. Upscaling is performed in each realization and the flow model is run. No
283 Kalman filtering is performed.

284 Cases A and B act as base cases to be used for comparison when the piezometric head
285 data are assimilated through the EnKF.

286 Case C is conditional to piezometric heads. The same 200 coarse realizations from Case
287 A serve as the initial ensemble of realizations to be used by the EnKF to assimilate the
288 piezometric head measurements from locations W1 to W9 for the first 60 time steps (66.7
289 days).

290 Case D is conditional to both logconductivity and piezometric heads. The same 200
291 coarse realizations from Case B serve as the initial ensemble of realizations to be used by
292 the EnKF to assimilate the piezometric head measurements from locations W1 to W9 for
293 the first 60 time steps (66.7 days).

294 In Cases C and D we use the measured heads obtained at the fine scale in the reference
295 realization as if they were measurements obtained at the coarse scale. There is an error
296 in this assimilation that we incorporate into the measurement error covariance matrix.
297 Specifically we here assumed a diagonal error covariance matrix, with all the diagonal

298 terms equal to 0.0025 m^2 ; this value is approximately equal to the average dispersion
 299 variance of the fine scale piezometric heads within the coarse scale blocks.

3.4. Performance Measurements

300 Since this is a synthetic experiment, the “true” aquifer response, evaluated at the fine
 301 scale, is known. We also know the upscaled conductivity tensors for the reference aquifer,
 302 which we will use to evaluate the performance of the updated conductivity tensors pro-
 303 duced by the EnKF.

304 The following criteria, some of which are commonly applied for optimal design evalua-
 305 tion [Nowak, 2010], will be used to analyze the performance of the proposed method and
 306 the worth of data:

- 307 1. Ensemble mean map. (It should capture the main patterns of variability of the
 308 reference map.)
- 309 2. Ensemble variance map. (It gives an estimate of the precision of the maps.)
3. Ensemble average absolute bias map, ϵ_X , made up by:

$$\epsilon_{X_i} = \frac{1}{N_e} \sum_{r=1}^{N_e} |X_{i,r} - X_{i,ref}|, \quad (14)$$

310 where X_i is the parameter being analyzed, at location i , $X_{i,r}$ represents its value for
 311 realization r , $X_{i,ref}$ is the reference value at location i , and N_e is the number of realizations
 312 of the ensemble (200, in this case). (It gives an estimate of the accuracy of the maps.)

4. Average absolute bias

$$AAB(X) = \frac{1}{N_b} \sum_{i=1}^{N_b} \epsilon_{X_i}, \quad (15)$$

313 where N_b is the number of interblocks when X is coarse logconductivity tensor component,
 314 or the number of blocks when X is piezometric head. (It gives a global measure of
 315 accuracy.)

5. Square root of the average ensemble spread

$$AESP(X) = \left[\frac{1}{N_b} \sum_{i=1}^{N_b} \sigma_{X_i}^2 \right]^{1/2}, \quad (16)$$

316 where $\sigma_{X_i}^2$ is the ensemble variance at location i . (It gives a global measure of precision.)

317 6. Comparison of the time evolution of the piezometric heads at the conditioning
 318 piezometers W1 to W9, and at the control piezometers W10 to W13. (It evaluates the
 319 capability of the EnKF to update the forecasted piezometric heads using the measured
 320 values.)

4. Discussion

321 Ensembles of coarse realizations for the four cases have been generated according to
 322 the conditions described earlier. Figure 8 shows the evolution of the piezometric heads in
 323 piezometers W1 and W9 for the 500 days of simulation; the first 60 steps (66.7 days) were
 324 used for conditioning in cases C and D. Similarly, Figure 9 shows piezometers W10 and
 325 W13; these piezometers were not used for conditioning. Figure 10 shows the ensemble
 326 mean and variance of the piezometric heads at the 60th time step, while Figure 11 shows
 327 the ensemble average absolute bias. Figure 12 shows the ensemble mean and variance of
 328 $\ln(K_{max})$ for interblocks between rows, and Figure 13 shows the ensemble average absolute
 329 bias. Finally, Table 2 shows the metric performance measurements for $\ln(K_{max})$ between
 330 rows and for piezometric heads at the 30th, 60th and 90th time steps.

4.1. The EnKF Coupled with Upscaling

331 The EnKF has the objective of updating conductivity realizations so that the solution
332 of the flow equation on the updated fields will match the measured piezometric heads.
333 Analyzing cases C and D in Figure 8, we can observe how the updated fields, when
334 piezometric head is assimilated by the EnKF, produce piezometric head predictions that
335 reproduce the measured values very well, particularly when compared with case A, which
336 corresponds to the case in which no conditioning data are considered. Notice also that
337 piezometric head data are assimilated only for the first 66.7 days (the period in which the
338 heads are almost perfectly reproduced in the EnKF updated fields) while the rest of the
339 simulation period serves as validation. Additional validation of the EnKF generated real-
340 izations is given in Figure 9 that shows two of the piezometers not used for conditioning;
341 we can also observe the improvement in piezometric head reproduction for cases C and D
342 as compared to case A. Furthermore, the analysis of Figure 10 shows how, for cases C and
343 D, the average spatial distribution, at the end of time step 60, follows closely the reference
344 piezometric head distribution, while the ensemble variance is reduced to very small values
345 everywhere. The ensemble average head bias is also noticeably reduced when conditioning
346 to heads, not just at the conditioning locations (as expected) but also elsewhere. A final
347 analysis to show how conditioning to the heads improves the overall reproduction of the
348 head spatial distribution is by looking at the metrics displayed in Table 2. Comparing
349 cases B and C, it is interesting to notice the increasing impact of the conditioning to
350 piezometric heads as time passes; at time step 30, the initial effect of just conditioning to
351 hydraulic conductivity measurements (which occurs from time step 0) is still larger than
352 just conditioning to the heads measured during the first 30 time steps, but at time step
353 60, this effect is clearly reversed, and it is maintained to time step 90 even though the

354 heads between steps 60 and 90 are not used for conditioning. As expected, conditioning
355 to both piezometric heads and hydraulic conductivities gives the best results in terms of
356 smallest bias and smallest spread.

357 From this analysis we conclude that the EnKF coupled with upscaling is able to generate
358 an aquifer model at a scale two orders of magnitude coarser than the reference aquifer
359 scale that is conditional to the piezometric heads.

360 Besides achieving the original goal of the EnKF algorithm, it is also important to
361 contrast the final conductivity model given by the EnKF, with the reference aquifer model.
362 For this purpose we will compare the final ensemble of realizations obtained for cases
363 C and D with the upscaled realization obtained from the reference, fine scale aquifer
364 model. Conditioning to piezometric head data should improve the characterization of
365 the logconductivities. Indeed, this is what happens as it can be seen when analyzing
366 Figures 12 and 13 and Table 2. In these figures only the maximum component of the
367 logconductivity tensors for the interblocks between rows is displayed, but the members
368 of the triplet for the tensor between rows, as well as the members of the triplet for the
369 tensors between columns, show a similar behavior. The ensemble mean maps are closer
370 to the reference map in case that conditioning data are used; the variance maps display
371 smaller values as compared to case A; and the bias map shows values closer to zero than in
372 case A. All in all, we can conclude that the EnKF updates the block conductivity tensors
373 to produce realizations which get closer to the aquifer model obtained after upscaling the
374 reference aquifer.

375 There remains the issue of conditioning to the fine scale conductivity measurements.
376 Since the fine scale conductivity measurements were used to condition the fine scale real-

377 izations, the conditioning should be noticed in the upscaled model only if the correlation
378 scale of the conductivity measurements is larger than the upscaled block size. In such a
379 case (as is the case for the example), the ensemble variance of the upscaled block con-
380 ductivity values should be smaller for blocks close to conditioning datum locations than
381 for those away from the conditioning points. Otherwise, if the correlation length is much
382 smaller than the block size, then all blocks have a variance reduction of the same magni-
383 tude and the impact of the conditioning data goes unnoticed. Case B is conditioned only
384 on the fine scale logconductivity measurements. Comparing cases A and B in Figure 12
385 and in Table 2 we notice that for the unconditional case, the ensemble mean of $\ln(K_{max})$
386 between rows is spatially homogeneous and so is the variance; however, as soon as the
387 fine scale conductivity data are used for the generation of the fine scale realizations, the
388 ensemble of upscaled realizations displays the effects of such conditioning, the ensem-
389 ble mean starts to show patterns closer to the patterns in the upscaled reference field
390 (Figure 7), and the ensemble variance becomes smaller for the interblocks closer to the
391 conditioning measurements. Analyzing case D in Figure 12, which takes the ensemble of
392 realizations from case B and updates it by assimilating the piezometric head measurements
393 at piezometers W1 to W9, we conclude that the initial conditioning effect (to hydraulic
394 conductivity data) is reinforced by the new conditioning data, the patterns observed in
395 the ensemble mean maps are even closer to the patterns in the reference realization, and
396 the ensemble variance remains small close to logconductivity conditioning locations and,
397 overall, is smaller than for case B.

398 Finally, when no conductivity data are used to condition the initial ensemble of re-
399 alizations, conditioning to piezometric heads through EnKF also serves to improve the

400 characterization of the logconductivities as can be seen analyzing case C in Figure 12 and
401 Table 2. Some patterns of the spatial variability of $\ln(K_{max})$ are captured by the ensem-
402 ble mean and the ensemble variance is reduced with respect to the unconditional case,
403 although in a smaller magnitude than when logconductivity data are used for conditioning.

404 From this analysis we conclude that conditioning to piezometric head data by the EnKF
405 coupled with upscaling improves the characterization of aquifer logconductivities whether
406 conductivity data are used for conditioning or not.

407 It should be emphasized that, since the EnKF algorithm starts after the upscaling of
408 the ensemble of fine scale realizations ends, the EnKF-coupled-with-upscaling performance
409 will be much restricted by the quality of the upscaling algorithm. It is important to use
410 as accurate an upscaling procedure as possible in the first step of the process, otherwise
411 the EnKF algorithm may fail. An interesting discussion on the importance of the choice
412 of upscaling can be read in the study of the MADE site by *Li et al.* [2011a].

4.2. Worth of Data

413 We can use the results obtained to make a quick analysis of the worth of data in
414 aquifer characterization, which confirms earlier findings [e.g., *Capilla et al.*, 1999; *Wen*
415 *et al.*, 2002; *Hendricks Franssen*, 2001; *Hendricks Franssen et al.*, 2003; *Fu and Gómez-*
416 *Hernández*, 2009; *Li et al.*, 2011c] and serves to show that the proposed approach works
417 as expected. By analyzing Figures 8, 9, 10, 11, 12, and 13, and Table 2, we can conclude
418 that conditioning to any type of data improves the characterization of the aquifer conduc-
419 tivities, and improves the characterization of the state of the aquifer (i.e., the piezometric
420 heads). The largest improvement occurs when both, hydraulic conductivity and piezo-
421 metric head measurements are used. These improvements can be seen qualitatively on

422 the ensemble mean maps, which are able to display patterns closer to those in the ref-
423 erence maps; on the ensemble variance maps, which display smaller values than for the
424 unconditional case; and on the ensemble average bias maps, which also show reduced bias
425 when compared with the unconditional case. Quantitatively, the same conclusions can be
426 made by looking at the metrics in the Table. The reproduction of the piezometric heads
427 also improves when conditioning to any type of data.

428 It is also interesting to analyze the trade-off between conductivity data and piezometric
429 head data by comparing cases B and C. As expected, the characterization of the spatial
430 variability of hydraulic conductivity is better when conductivity data are used for con-
431 ditioning than when piezometric head are; also, as expected, the opposite occurs for the
432 characterization of the piezometric heads.

4.3. Other Issues

433 We have chosen a relatively small-sized fine scale model to demonstrate the method-
434 ology, since we needed the solution at the fine scale to create the sets of conditioning
435 data and to verify that the coarse scale models generated by the proposed approach give
436 good approximations of the “true” response of the fine scale aquifer. We envision that the
437 proposed approach should be used only when the implementation of the numerical model
438 and the EnKF are impractical at the fine scale.

439 To our understanding, it is the first time that the EnKF is applied on an aquifer with
440 conductivities characterized by full tensors. The approach of representing the tensors by
441 their invariants seems to work in this context. More sophisticated EnKF implementations,
442 such as double ensemble Kalman filter [*Houtekamer and Mitchell, 1998*], ensemble square
443 root filter [*Whitaker and Hamill, 2002*], Kalman filter based on the Karhunen-Loeve de-

444 composition [Zhang *et al.*, 2007], normal-score ensemble Kalman filter [Zhou *et al.*, 2011b],
445 could have been used, which would have worked equally well or better than the standard
446 EnKF.

447 The example has been demonstrated using a reference conductivity field that was gener-
448 ated following a multiGaussian stationary random function. Could the method be applied
449 to other types of random functions, i.e., non-multiGaussian or non-stationary? It could,
450 as long as each step of the approach (see Section 2) could. More precisely, for the first
451 step, the generation of the fine scale hydraulic conductivity measurements, there are al-
452 ready many algorithms that can generate realizations from a wide variety of random
453 functions, including non-multiGaussian and non-stationary; the second step is basically
454 deterministic, we replace an assembly of heterogeneous values by an equivalent block ten-
455 sor, the underlying random function used to generate the fine scale realizations has no
456 interference on the upscaling; however, for the third step, the application of EnKF to
457 non-multiGaussian parameter fields is more difficult, some researchers propose moving on
458 to particle filtering [Arulampalam *et al.*, 2002], some others have worked on variants of
459 the EnKF to handle the non-multiGaussianity [e.g., Sun *et al.*, 2009; Zhou *et al.*, 2011b;
460 Schöniger *et al.*, 2011; Li *et al.*, 2011d]; the non-stationarity is not an issue, since the
461 EnKF deals, by construction, with non-stationary states.

5. Conclusion

462 The “missing scale” issue brought out by Tran [1996] is still, today, much overlooked.
463 Data, particularly conductivity data, are collected at smaller support volumes and in
464 larger quantities than years ago, yet, when constructing a numerical model based on

465 these data, the discrepancy between the scale at which data are collected and the scale of
466 the numerical model is most often disregarded.

467 We have presented an approach to rigorously account for fine-scale conductivity mea-
468 surements on coarse-scale conditional inverse modeling. The resulting model is composed
469 of an ensemble of realizations of conductivity tensors at a scale (much) coarser than the
470 scale at which conductivities were measured. The ensemble of final realizations is condi-
471 tioned to both conductivity and piezometric head measurements. The latter conditioning
472 is achieved by using the ensemble Kalman filter on realizations of conductivity tensors.
473 To handle the tensor parameters, we propose to work with the invariants of the tensors,
474 instead of their representations on a specific reference system, this approach allows the
475 ensemble Kalman filter to perform a tensor updating which produces realizations that are
476 conditioned to the transient piezometric head measurements.

477 **Acknowledgments.** The authors acknowledge three anonymous reviewers and Wolf-
478 gang Nowak for their comments on the previous versions of the manuscript, which helped
479 substantially in improving the final version. The authors gratefully acknowledge the fi-
480 nancial support by ENRESA (project 0079000029). Extra travel Grants awarded to the
481 first and second authors by the Ministry of Education (Spain) are also acknowledged. The
482 second author also acknowledges the financial support from China Scholarship Council.

References

483 Aanonsen, S. L., G. Naevdal, D. S. Oliver, A. C. Reynolds, and B. Valles (2009), Ensemble
484 kalman filter in reservoir engineering - a review, *SPE Journal*, 14(3), 393–412.

- 485 Arulampalam, M. S., S. Maskell, N. Gordon, and T. Clapp (2002), A tutorial on parti-
486 cle filters for online nonlinear/non-Gaussian Bayesian tracking, *IEEE Transactions on*
487 *signal processing*, 50(2), 174–188.
- 488 Bear, J. (1972), *Dynamics of fluids in porous media.*, American Elsevier Pub. Co., New
489 York.
- 490 Behrens, R., M. MacLeod, T. Tran, and A. Alimi (1998), Incorporating seismic attribute
491 maps in 3D reservoir models, *SPE Reservoir Evaluation & Engineering*, 1(2), 122–126.
- 492 Burgers, G., P. van Leeuwen, and G. Evensen (1998), Analysis scheme in the ensemble
493 Kalman filter, *Monthly Weather Review*, 126, 1719–1724.
- 494 Capilla, J., and C. Llopis-Albert (2009), Gradual conditioning of non-Gaussian transmis-
495 sivity fields to flow and mass transport data: 1. Theory, *Journal of Hydrology*, 371(1-4),
496 66–74.
- 497 Capilla, J. E., J. Rodrigo, and J. J. Gómez-Hernández (1999), Simulation of non-gaussian
498 transmissivity fields honoring piezometric data and integrating soft and secondary in-
499 formation, *Math. Geology*, 31(7), 907–927.
- 500 Carrera, J., A. Alcolea, A. Medina, J. Hidalgo, and L. Slooten (2005), Inverse problem in
501 hydrogeology, *Hydrogeology Journal*, 13(1), 206–222.
- 502 Chen, Y., and D. Zhang (2006), Data assimilation for transient flow in geologic formations
503 via ensemble Kalman filter, *Advances in Water Resources*, 29(8), 1107–1122.
- 504 Deutsch, C. V., and A. G. Journel (1998), *GSLIB, Geostatistical Software Library and*
505 *User’s Guide*, second ed., Oxford University Press, New York.
- 506 Durlofsky, L. J., R. C. Jones, and W. J. Milliken (1997), A nonuniform coarsening ap-
507 proach for the scale-up of displacement processes in heterogeneous porous media, *Adv.*

508 *in Water Resour.*, 20(5-6), 335–347.

509 Evensen, G. (2003), The ensemble Kalman filter: Theoretical formulation and practical
510 implementation, *Ocean dynamics*, 53(4), 343–367.

511 Freeze, R. A., and J. A. Cherry (1979), *Groundwater*, Prentice-Hall.

512 Fu, J., and J. Gómez-Hernández (2009), Uncertainty assessment and data worth in
513 groundwater flow and mass transport modeling using a blocking Markov chain Monte
514 Carlo method, *Journal of Hydrology*, 364(3-4), 328–341.

515 Fu, J., H. A. Tchelepi, and J. Caers (2010), A multiscale adjoint method to compute sensi-
516 tivity coefficients for flow in heterogeneous porous media, *Advances in Water Resources*,
517 33(6), 698–709, doi:10.1016/j.advwatres.2010.04.005.

518 Gómez-Hernández, J. J. (1991), A stochastic approach to the simulation of block conduc-
519 tivity values conditioned upon data measured at a smaller scale, Ph.D. thesis, Stanford
520 University.

521 Gómez-Hernández, J. J., and A. G. Journel (1993), Joint sequential simulation of multi-
522 Gaussian fields, *Geostatistics Troia*, 92(1), 85–94.

523 Gómez-Hernández, J. J., and R. M. Srivastava (1990), ISIM3D: an ANSI-C three dimen-
524 sional multiple indicator conditional simulation program, *Computers & Geosciences*,
525 16(4), 395–440.

526 Gómez-Hernández, J. J., A. Sahuquillo, and J. E. Capilla (1997), Stochastic simulation of
527 transmissivity fields conditional to both transmissivity and piezometric data, 1, Theory,
528 *Journal of Hydrology*, 203(1–4), 162–174.

529 Guadagnini, A., and S. P. Neuman (1999), Nonlocal and localized analyses of conditional
530 mean steady state flow in bounded, randomly nonuniform domains: 1. theory and

- 531 computational approach, *Water Resour. Res.*, *35*(10), 2999–3018.
- 532 Hendricks Franssen, H. (2001), Inverse stochastic modelling of groundwater flow and mass
533 transport, Ph.D. thesis, Technical University of Valencia.
- 534 Hendricks Franssen, H., and W. Kinzelbach (2009), Ensemble Kalman filtering versus
535 sequential self-calibration for inverse modelling of dynamic groundwater flow systems,
536 *Journal of Hydrology*, *365*(3-4), 261–274.
- 537 Hendricks Franssen, H., A. Alcolea, M. Riva, M. Bakr, N. van der Wiel, F. Stauffer, and
538 A. Guadagnini (2009), A comparison of seven methods for the inverse modelling of
539 groundwater flow. application to the characterisation of well catchments, *Advances in*
540 *Water Resources*, *32*(6), 851–872, doi:10.1016/j.advwatres.2009.02.011.
- 541 Hendricks Franssen, H. J., J. J. Gómez-Hernández, and A. Sahuquillo (2003), Coupled in-
542 verse modelling of groundwater flow and mass transport and the worth of concentration
543 data, *Journal of Hydrology*, *281*(4), 281–295.
- 544 Houtekamer, P., and H. Mitchell (1998), Data assimilation using an ensemble kalman
545 filter technique, *Monthly Weather Review*, *126*(3), 796–811.
- 546 Hu, L. Y. (2000), Gradual deformation and iterative calibration of gaussian-related
547 stochastic models, *Math. Geology*, *32*(1), 87–108.
- 548 Indelman, P., and B. Abramovich (1994), Nonlocal properties of nonuniform averaged
549 flows in heterogeneous media, *Water Resour. Res.*, *30*(12), 3385–3393.
- 550 Li, L., H. Zhou, and J. J. Gómez-Hernández (2010), Steady-state groundwater flow mod-
551 eling with full tensor conductivities using finite differences, *Computers & Geosciences*,
552 *36*(10), 1211–1223.

- 553 Li, L., H. Zhou, and J. J. Gómez-Hernández (2011a), A comparative study of
554 three-dimensional hydraulic conductivity upscaling at the macrodispersion experiment
555 (MADE) site, columbus air force base, mississippi (USA), *Journal of Hydrology*, *404*(3-
556 4), 135–142.
- 557 Li, L., H. Zhou, and J. J. Gómez-Hernández (2011b), Transport upscaling using multi-
558 rate mass transfer in three-dimensional highly heterogeneous porous media, *Advances*
559 *in Water Resources*, *34*(4), 478–489.
- 560 Li, L., H. Zhou, J. J. Gómez-Hernández, and H. J. Hendricks Franssen (2011c), Jointly
561 mapping hydraulic conductivity and porosity by assimilating concentration data via
562 ensemble kalman filter, *Journal of Hydrology*, p. submitted.
- 563 Li, L., H. Zhou, H. J. Hendricks Franssen, and J. J. Gómez-Hernández (2011d), Ground-
564 water flow inverse modeling in non-multigaussian media: performance assessment of the
565 normal-score ensemble kalman filter, *Hydrology and Earth System Sciences Discussions*,
566 *8*(4), 6749–6788, doi:10.5194/hessd-8-6749-2011.
- 567 Mariethoz, G., P. Renard, and J. Straubhaar (2010), The direct sampling method to per-
568 form multiple-point geostatistical simulaitons, *Water Resources Research*, *46*, W11,536,
569 doi:10.1029/2008WR007621.
- 570 McLaughlin, D., and L. Townley (1996), A reassessment of the groundwater inverse prob-
571 lem, *Water Resources Research*, *32*(5), 1131–1161.
- 572 Naevdal, G., L. Johnsen, S. Aanonsen, and E. Vefring (2005), Reservoir monitoring and
573 continuous model updating using ensemble kalman filter, *SPE Journal*, *10*(1).
- 574 Nowak, W. (2010), Measures of parameter uncertainty in geostatistical estimation and
575 geostatistical optimal design, *Math. Geology*, *49*, 199–221.

- 576 Oliver, D., and Y. Chen (2011), Recent progress on reservoir history matching: a review,
577 *Computational Geosciences*, 15(1), 185–221.
- 578 Peters, L., R. J. Arts, G. K. Brower, C. R. Geel, S. Cullick, R. J. Lorentzen, Y. Chen,
579 N. Dunlop, F. Vossepoel, R. Xu, P. Sarman, A. A. H. H., and A. Reynolds (2010),
580 Results of the brugge benchmark study for flooding optimization and history matching,
581 *SPE Reservoir Evaluation & Engineering*, 13(3), 391–405, doi:10.2118/119094-PA.
- 582 Renard, P., and G. de Marsily (1997), Calculating equivalent permeability: A review,
583 *Advances in Water Resources*, 20(5-6), 253–278.
- 584 Rubin, Y., and J. J. Gómez-Hernández (1990), A stochastic approach to the problem
585 of upscaling of conductivity in disordered media, theory and unconditional numerical
586 simulations, *Water Resour. Res.*, 26(4), 691–701.
- 587 Sánchez-Vila, X., J. Girardi, and J. Carrera (1995), A synthesis of approaches to upscaling
588 of hydraulic conductivities, *Water Resources Research*, 31(4), 867–882.
- 589 Sánchez-Vila, X., A. Guadagnini, and J. Carrera (2006), Representative hydraulic
590 conductivities in saturated groundwater flow, *Reviews of Geophysics*, 44(3), doi:
591 10.1029/2005RG000169.
- 592 Schöniger, A., W. Nowak, and H. J. Hendricks Franssen (2011), Parameter estimation by
593 ensemble Kalman filters with transformed data: approach and application to hydraulic
594 tomography, p. submitted to Water Resources Research.
- 595 Strebelle, S. (2002), Conditional simulation of complex geological structures using
596 multiple-point statistics, *Mathematical Geology*, 34(1), 1–21.
- 597 Sun, A. Y., A. P. Morris, and S. Mohanty (2009), Sequential updating of multimodal
598 hydrogeologic parameter fields using localization and clustering techniques, *Water Re-*

599 *sources Research*, 45, 15 PP.

600 Tran, T. (1996), The ‘missing scale’ and direct simulation of block effective properties,
601 *Journal of Hydrology*, 183(1-2), 37–56, doi:10.1016/S0022-1694(96)80033-3.

602 Tran, T., X. Wen, and R. Behrens (1999), Efficient conditioning of 3D fine-scale reservoir
603 model to multiphase production data using streamline-based coarse-scale inversion and
604 geostatistical downscaling, in *SPE Annual Technical Conference and Exhibition*.

605 Tureyen, O., and J. Caers (2005), A parallel, multiscale approach to reservoir modeling,
606 *Computational Geosciences*, 9(2), 75–98.

607 Wen, X. H., and J. J. Gómez-Hernández (1996), Upscaling hydraulic conductivities: An
608 overview, *J. of Hydrology*, 183(1-2), ix–xxxii.

609 Wen, X. H., C. Deutsch, and A. Cullick (2002), Construction of geostatistical aquifer
610 models integrating dynamic flow and tracer data using inverse technique, *Journal of*
611 *Hydrology*, 255(1-4), 151–168.

612 Whitaker, J., and T. Hamill (2002), Ensemble data assimilation without perturbed ob-
613 servations, *Monthly Weather Review*, 130(7), 1913–1925.

614 White, C. D., and R. N. Horne (1987), Computing absolute transmissibility in the presence
615 of Fine-Scale heterogeneity, *SPE 16011*.

616 Yeh, W. (1986), Review of parameter identification procedures in groundwater hydrology:
617 The inverse problem, *Water Resources Research*, 22(2), 95–108.

618 Zhang, D., Z. Lu, and Y. Chen (2007), Dynamic reservoir data assimilation with an
619 efficient, dimension-reduced kalman filter, *SPE Journal*, 12(1), 108–117.

620 Zhou, H., L. Li, and J. J. Gómez-Hernández (2010), Three-dimensional hydraulic conduc-
621 tivity upscaling in groundwater modelling, *Computers & Geosciences*, 36(10), 1224–

622 1235.

623 Zhou, H., J. J. Gómez-Hernández, and L. Li (2011a), Inverse methods in hydrogeology:
624 evolution and future trends, *Journal of Hydrology*, p. Submitted.

625 Zhou, H., J. J. Gómez-Hernández, H.-J. Hendricks Franssen, and L. Li (2011b), An
626 approach to handling Non-Gaussianity of parameters and state variables in ensemble
627 Kalman filter, *Advances in Water Resources*, *34*(7), 844–864.

628 Zimmerman, D., G. De Marsily, C. Gotway, M. Marietta, C. Axness, R. Beauheim,
629 R. Bras, J. Carrera, G. Dagan, P. Davies, et al. (1998), A comparison of seven geosta-
630 tistically based inverse approaches to estimate transmissivities for modeling advective
631 transport by groundwater flow, *Water Resources Research*, *34*(6), 1373–1413.

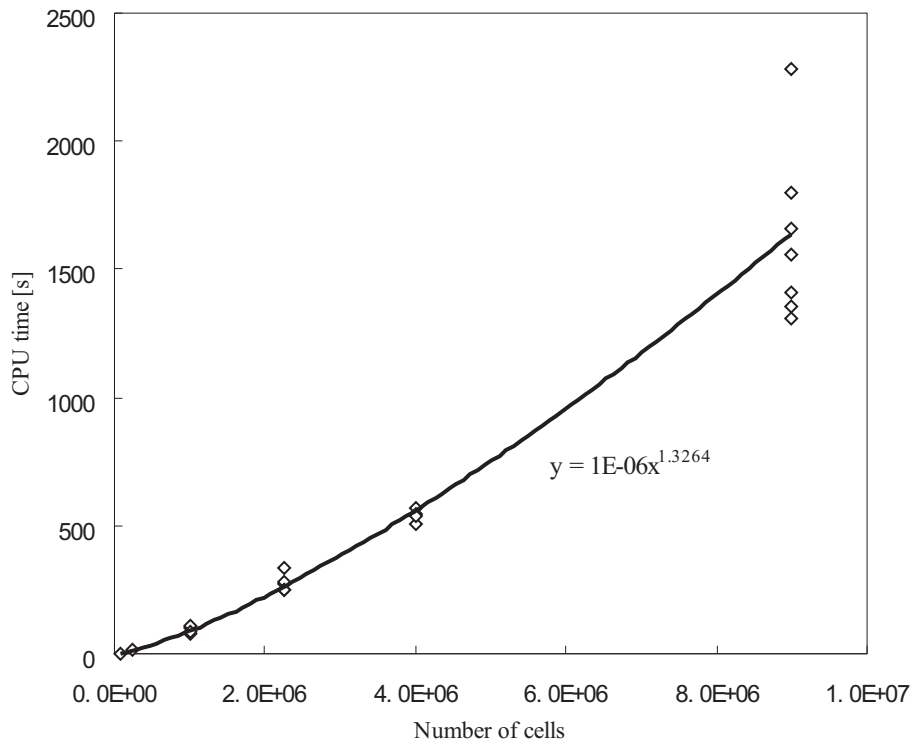


Figure 1. Regression of CPU time versus number of cells from several runs of MODFLOW on heterogeneous realizations.

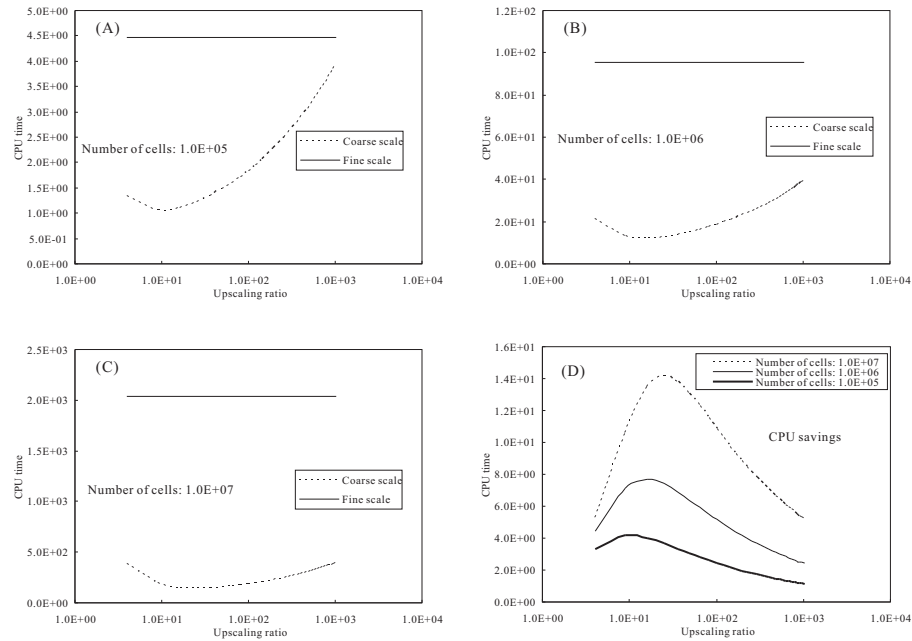


Figure 2. CPU time as a function of upscaling ratio for a single time step modeling. Plots A, B and C show, for different fine scale model sizes, the CPU time needed to run one single time step in a fine scale model and the CPU times needed for the upscaling plus running the flow model for different sizes of the upscaling block. Plot D shows the ratio of CPU time between the fine scale and the coarse scale, the larger the ratio, the larger the savings.

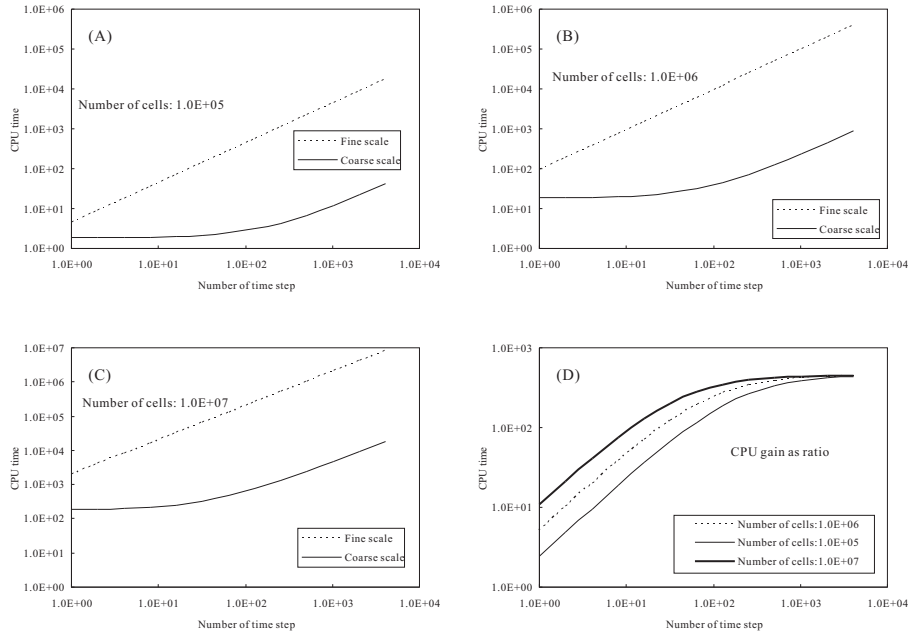


Figure 3. CPU time as a function of the number of time steps modeled. Plots A, B and C show, for a fine scale model of 10^5 nodes, and for an upscaled model of 10^3 blocks (upscaling ratio of 100), the CPU time needed to run the fine and coarse scale models as a function of the number of time steps. Plot D shows the ratio of CPU time between the fine scale and the coarse scale, the larger the ratio, the larger the savings.

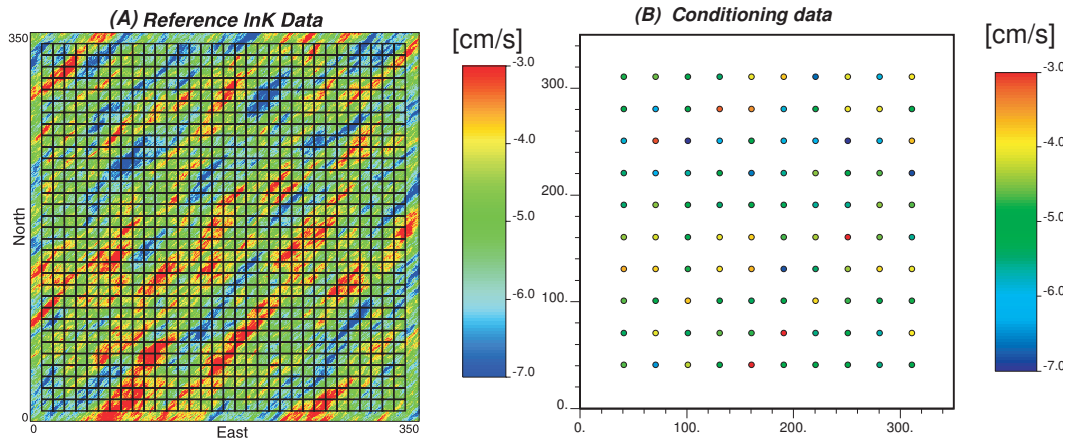


Figure 4. (A) Reference $\ln K$ field overlaid with the discretization of the numerical model at the coarse scale. (B) Conditioning $\ln K$ data.

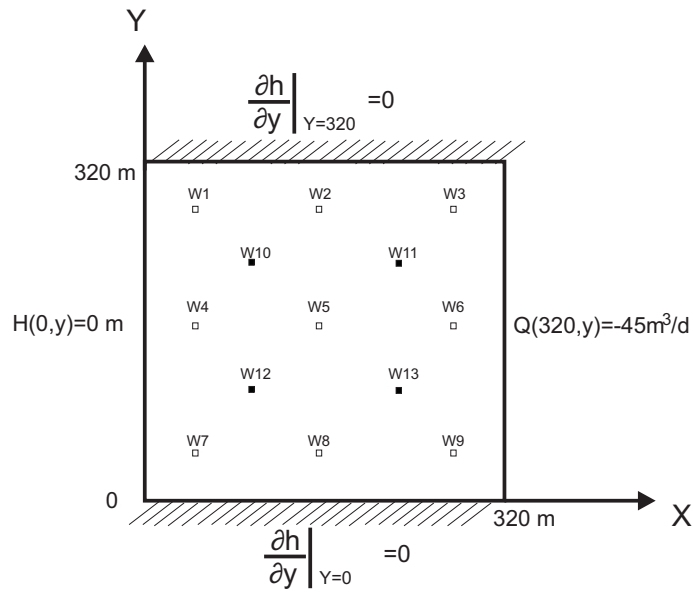


Figure 5. Sketch of the flow problem with boundary conditions, observation and prediction wells. Empty squares correspond to the piezometric head observation wells (W1-W9); filled squares correspond to the control wells (W10-W13).

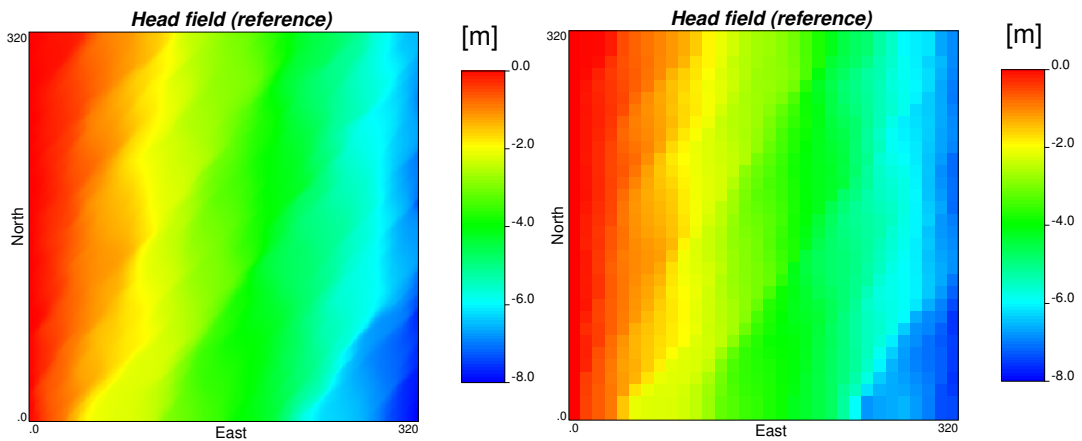


Figure 6. Reference piezometric head at the 60th time step. Left, as obtained at the fine scale; right, as obtained at the coarse scale

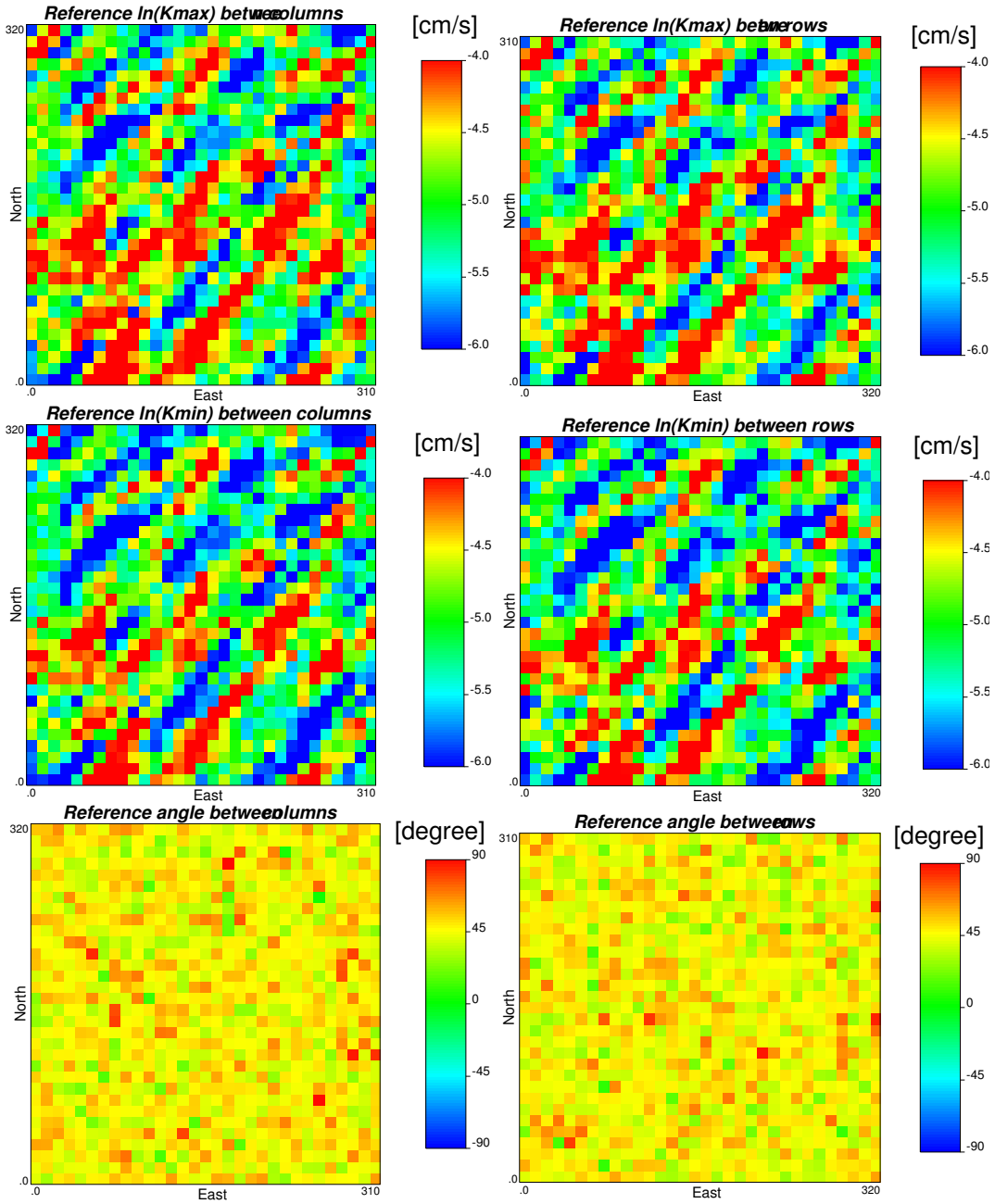


Figure 7. Upscaled values for the interblock tensor components: $\ln(K_{max})$, $\ln(K_{min})$ and rotation angle for the maximum component measured from the x -axis θ (in degrees), for both the interblocks between columns and the interblocks between rows. Upscaling method used: Laplacian with a skin of 10 m

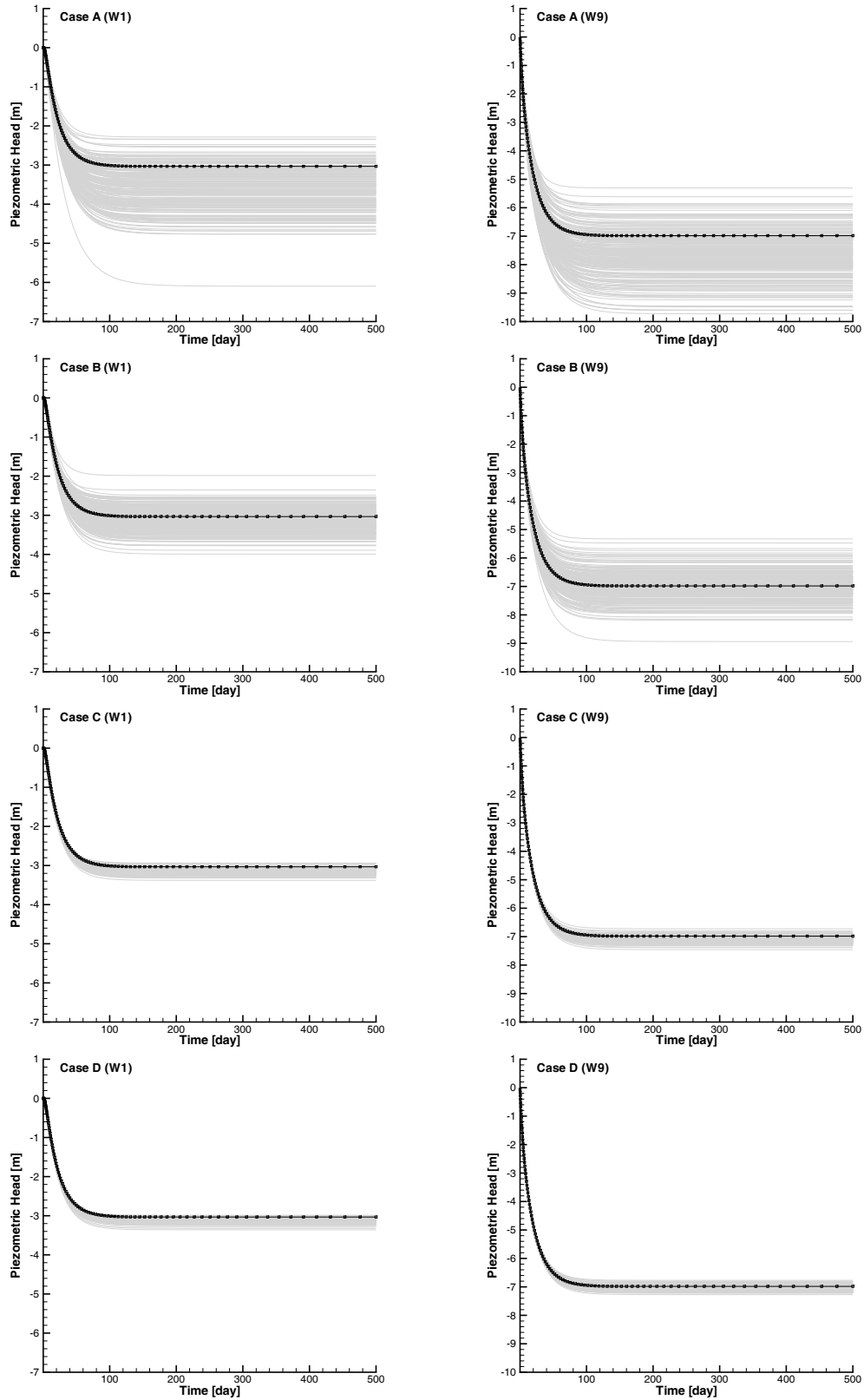


Figure 8. Piezometric head time series in the reference field and simulated ones for all cases at wells W1 (left column) and W9 (right column). The piezometric heads measured at these wells during the first 67.7 days were used as conditioning data for cases B and D.

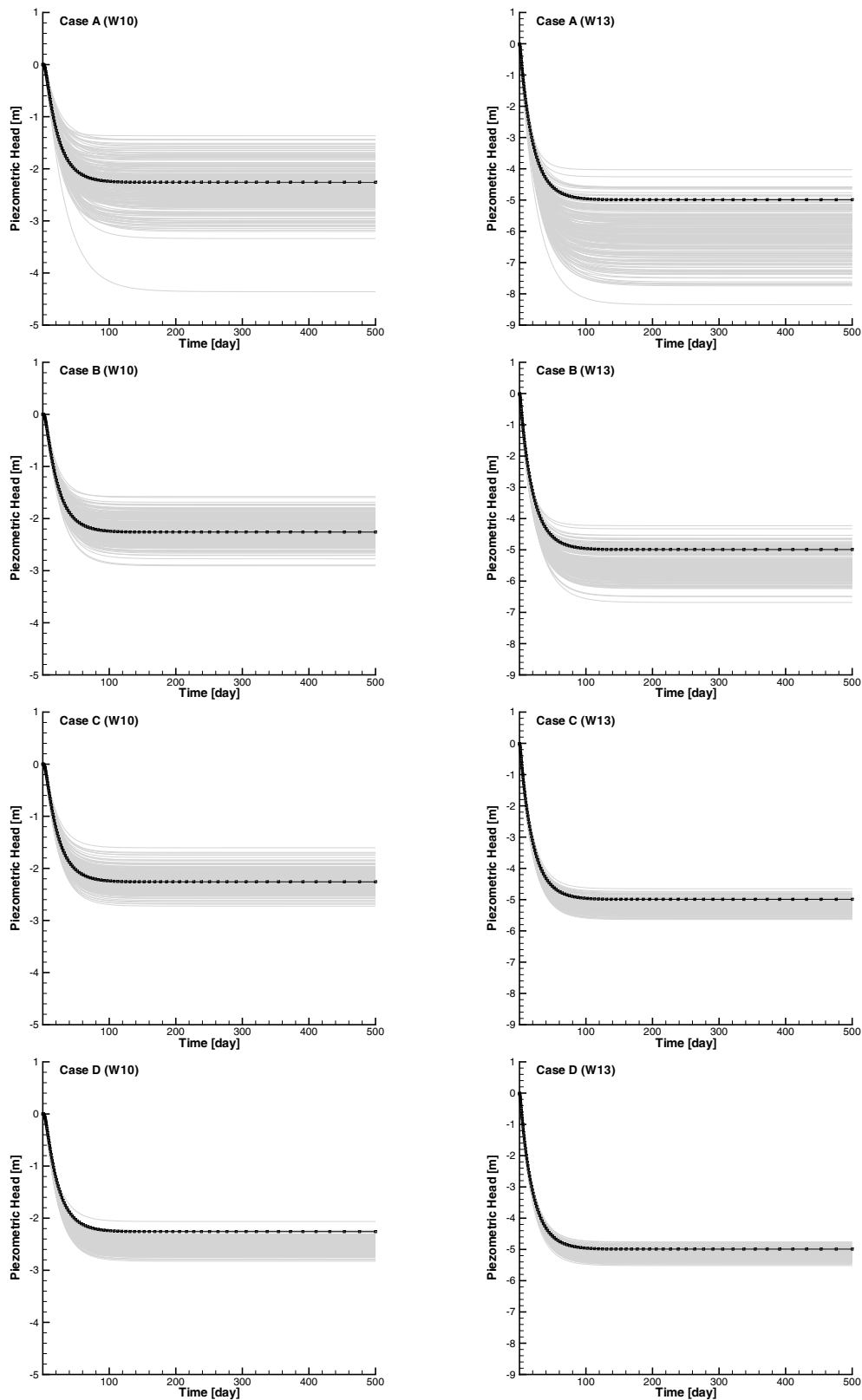


Figure 9. Piezometric head time series in the reference field and simulated ones for all cases at control wells W10 (left column) and W13 (right column). These wells were not used as conditioning data for any case.

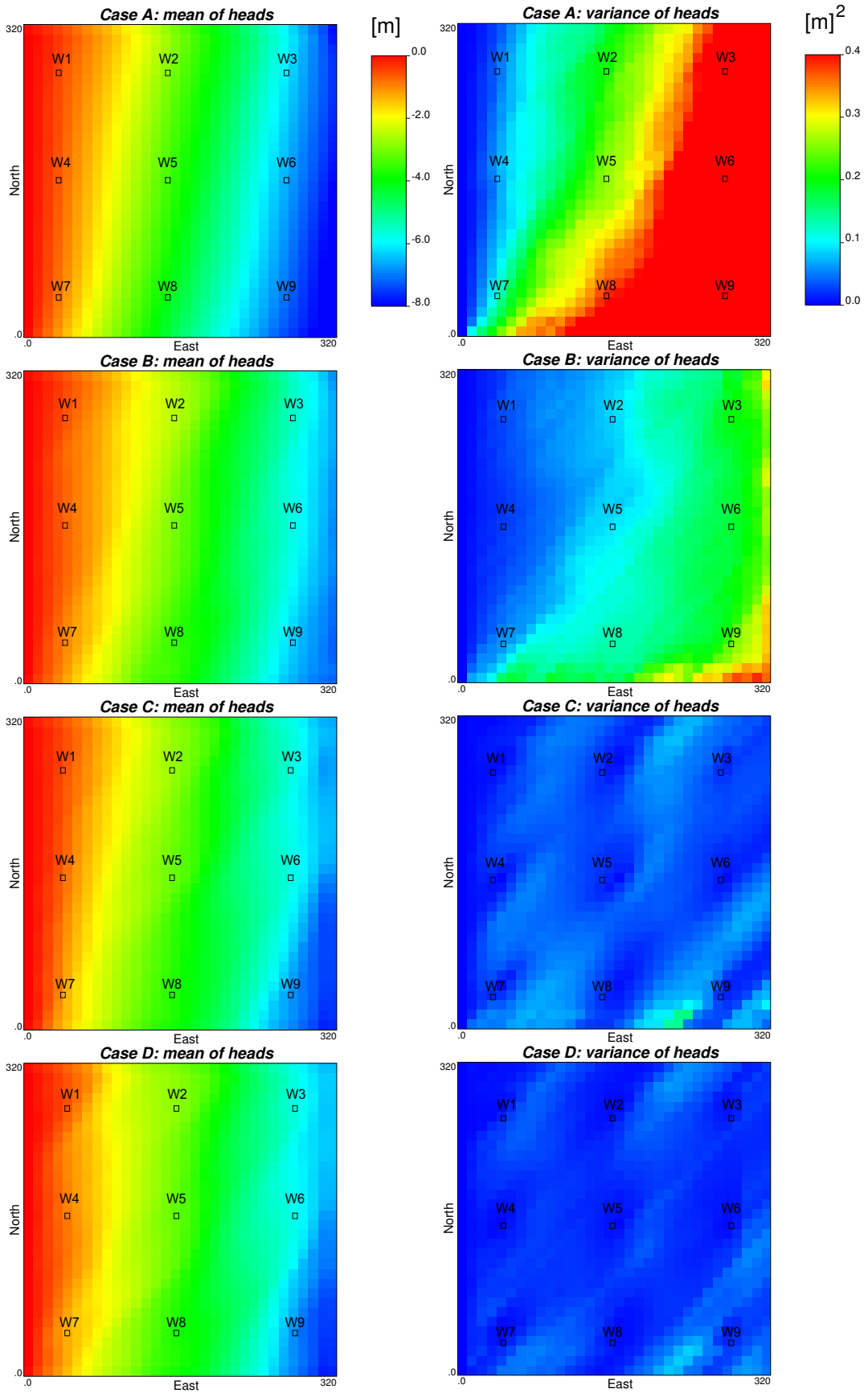


Figure 10. Ensemble average and variance of piezometric heads for the different cases.
 D R A F T November 18, 2011, 1:49pm D R A F T

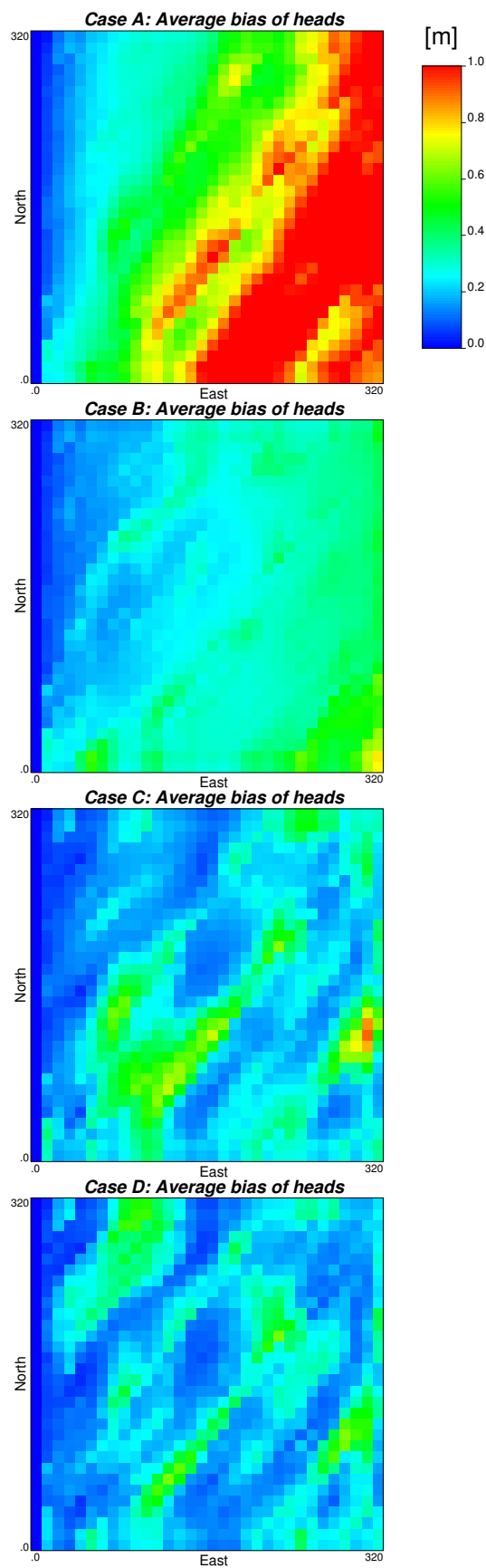


Figure 11. Ensemble average absolute bias of piezometric heads for the different cases.
D R A F T November 18, 2011, 1:49pm D R A F T

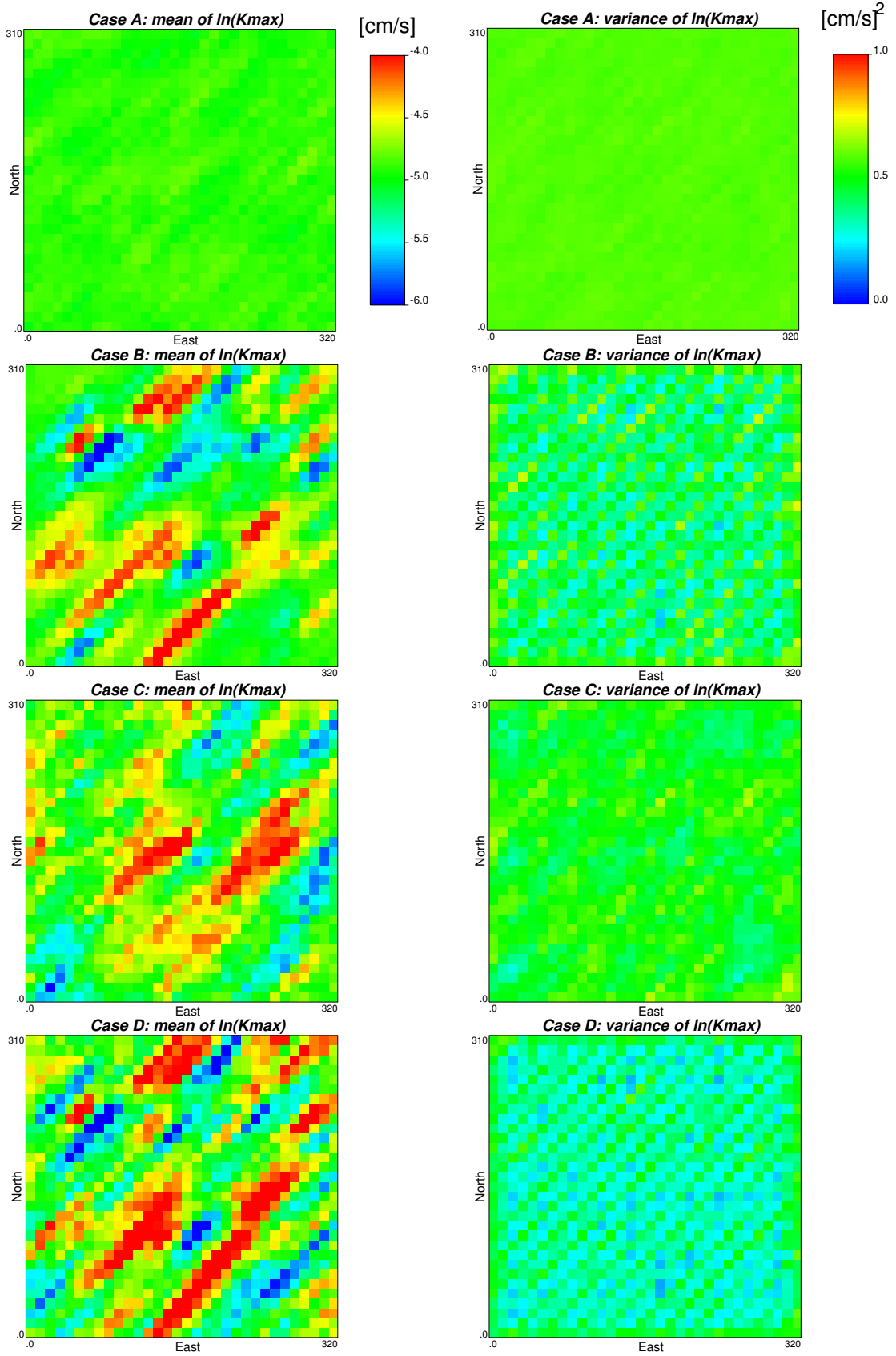


Figure 12. Ensemble average and variance of $\ln(K_{max})$ for the different cases.
 D R A F T November 18, 2011, 1:49pm

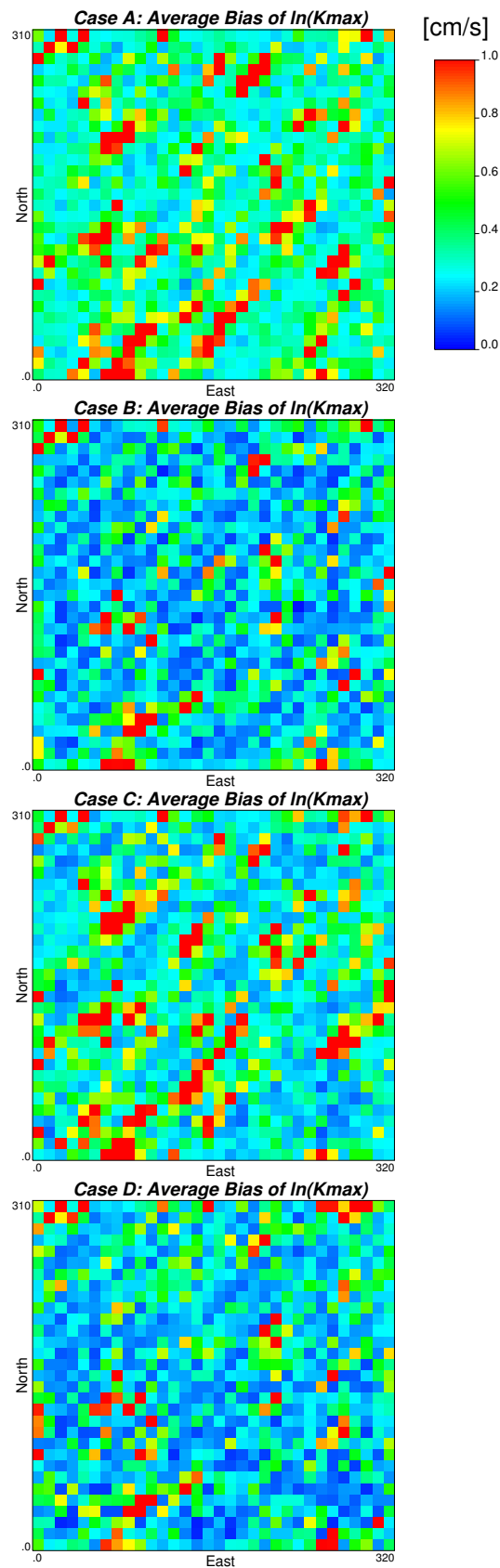


Figure 13. Ensemble average absolute bias of $\ln(K_{max})$ for the different cases.

Table 1. Definition of Cases depending on the the different sets of conditioning data.

Conditioning Data	Case A	Case B	Case C	Case D
Hydraulic conductivities(K)	No	Yes	No	Yes
Dynamic piezometric heads(h)	No	No	Yes	Yes

Table 2. Bias and spread of predicted heads at time steps 30, 60 and 90 and of updated loghydraulic conductivity $\ln K_{max}^{b,r}$ at time step 60.

	Case A	Case B	Case C	Case D
$AAB(h_{nt=30})$	0.189	0.119	0.124	0.118
$AESP(h_{nt=30})$	0.201	0.132	0.111	0.086
$AAB(h_{nt=60})$	0.580	0.256	0.224	0.195
$AESP(h_{nt=60})$	0.533	0.323	0.186	0.146
$AAB(h_{nt=90})$	0.672	0.281	0.236	0.204
$AESP(h_{nt=90})$	0.627	0.355	0.195	0.153
$AAB(\ln K_{max})$	0.452	0.306	0.417	0.296
$AESP(\ln K_{max})$	0.805	0.660	0.702	0.594